ON-LINE APPENDIX: MATERIALS AND METHODS

Classification of Heart Lesions

On the basis of the nature of the heart lesion and in utero blood flow, the preterm CHD cases were subsequently subdivided into 2 groups: a complex heart lesion cohort in which there was either lower PaO_2 and abnormal blood flow around the aortic arch, or simply lower PaO_2 with normal flow around the arch and a cohort of preterm neonates with CHD without complex lesions and/or compromised cerebral blood flood in utero. A secondary hypothesis was that preterm neonates with CHD with major in utero circulatory disturbances, like those with hypoplastic left heart syndrome, transposition of the great arteries, and certain right-sided heart lesions including Ebstein anomaly with significant valvular disturbance, would have abnormal cerebral microstructure relative to preterm neonates with other forms of CHD.

Determination of Term Control Subjects

Neonates without CHD were selected for inclusion in the comparison groups provided they had normal conventional and diffusion-weighted MR images and no history of chromosomal abnormalities, mitochondrial/metabolic diseases, treatment with extracorporeal membrane oxygenation, or significant neurologic abnormalities, including diffuse hypotonia/hypertonia, epilepsy, or significant neurodevelopmental disabilities. By identifying these neonates from the same neonatal intensive care units at the same tertiary care hospital, we were able to match our comparison groups to our target population on as many potentially confounding clinical variables as possible.

To assess how our comparison cohorts of critically ill preterm and term neonates without CHD compared with other populations of "healthy" preterm and term infants, we performed region-of-interest measurements in standardized brain regions on fractional anisotropy (FA) and diffusivity (axial diffusivity, AD; radial diffusivity, RD) maps reconstructed in DTIStudio (Johns Hopkins University, Baltimore, Maryland) and compared the values from our cohorts of critically ill neonates with published normative values.[1] The results indicated that the DTI measurements in this study were within range of published normative data (see below).

Neonatal TBSS Methods

DTI data analysis was performed with the use of FSL software (Version 4.1.4; http://www.fmrib.ox.ac.uk/fsl). Our protocol for neonatal TBSS was similar to other published methods.[2] The individual images were first corrected for head motion and eddy currents, followed by brain segmentation using FSL's Brain Extraction Tool. The diffusion tensors were then reconstructed to generate fractional anisotropy maps. To improve the success of registrations, each subject's FA map was first linearly registered to standard space and then nonlinearly aligned to every other subject to determine the image that best represented the cohort, deemed the one requiring the least average amount of warping. The nonlinear transformation to the best representative was then applied to all images, followed by affine alignment to Montreal Neurological Institute 152 standard space. A mean FA image of all subjects was then constructed, and this image was used as the registration target of all subsequent analyses. For each individual analysis, a mean FA skeleton was generated with a threshold at 0.18 to include major tracts in the neonatal brain, while removing peripheral tracts where added subject variability would deem the analysis uncertain. Additionally, the previously determined nonlinear warps were applied to each subject's mean diffusivity (MD), axial diffusivity, and radial diffusivity maps calculated using the Diffusion Toolbox in FMRIB, aligning them to the FA skeleton for analysis. Voxelwise statistics were performed with the use of Threshold-Free Cluster Enhancement (TFCE) and corrected for multiple comparisons, except where indicated.

As a secondary analysis, the best subject determined from the previous step was chosen as the template for the initial registration step to generate a mean FA map of the control group. Every other control subject's FA map was nonlinearly registered to the template with the use of FSL's FNIRT nonlinear registration tool, with the resulting transforms averaged to generate a mean FA image.

This image was then used as the template for the next iteration, and the process was repeated 4 times, at which point additional iterations yielded no further discernible improvement in the registration. TBSS was then performed between the cohorts of interest using the newly generated mean FA map as the template for registration. This step is essentially a fifth iteration of the procedure described above, this time including all subjects of interest to generate the FA skeleton. Mean FA skeleton was generated and threshold set at 0.18 as above, and voxel wise statistics performed using TFCE. We also manually placed ROIs directly on the FA and diffusivity maps generated in the DTIStudio; see next section below) to 1) validate the TBSS technique for use in this population and 2) provide quantitative DTI metrics for both white and gray matter regions, the latter of which cannot be evaluated by TBSS, which, in turn, were used for secondary analyses investigating potential relations between DTI metrics and clinical/intraoperative variables. Of note, there were 2 term controls, 3 preterm controls, and 3 preterm CHD cases that failed the registration mostly because of motion artifact and therefore were excluded from the original study cohort.

TBSS is a well-validated technique for evaluating white matter microstructure in adults and has been previously optimized for evaluating white matter microstructure in preterm neonates without CHD.[2] This is the first time TBSS has been used to assess white matter microstructure in preterm neonates with CHD. TBSS can create an objective and reproducible voxel-wise survey of central white matter tracts for revealing group differences. This technique avoids hypothesis-based section of white matter regions (ie, such as ROI or tractography), and the technique also avoids bias/subjective selection of tracts. We did supplement our work with ROI measurements, which did demonstrate similar

On-line Table: DTI manual ROI-based results comparing preterm neonates with CHD with high-risk term and preterm comparison groups

		Preterm (*n* = 27) Mean (SD)	Term (*n* = 28) Mean (SD)	Preterm CHD (*n* = 42) Mean (SD)	*P* Value[a]
Peripheral white matter					
Frontal[b]	FA	0.16 (0.06)	0.17 (0.06)	0.15 (0.07)	.551
	RA	0.13 (0.05)	0.14 (0.05)	0.13 (0.06)	.550
	Axial	1.89 (0.37)	1.74 (0.34)	1.81 (0.36)	.418
	Radial	1.52 (0.38)	1.36 (0.34)	1.46 (0.39)	.415
	ADC	1.64 (0.37)	1.49 (0.34)	1.58 (0.38)	.432
Parietal[b]	FA	0.17 (0.06)	0.18 (0.05)	0.17 (0.06)	.948
	RA	0.14 (0.05)	0.15 (0.04)	0.14 (0.06)	.953
	Axial	1.95 (0.33)	1.80 (0.35)	1.91 (0.40)	.378
	Radial	1.52 (0.33)	1.39 (0.31)	1.49 (0.38)	.492
	ADC	1.67 (0.33)	1.53 (0.32)	1.63 (0.38)	.475
Anterior[b]	FA	0.19 (0.07)	0.23 (0.07)	0.21 (0.10)	.426
	RA	0.16 (0.06)	0.19 (0.06)	0.17 (0.09)	.427
	Axial	1.88 (0.30)	1.72 (0.33)	1.80 (0.35)	.297
	Radial	1.43 (0.32)	1.24 (0.29)	1.37 (0.43)	.167
	ADC	1.58 (0.31)	1.40 (0.30)	1.52 (0.39)	.183
Middle[b]	FA	0.22 (0.08)	0.25 (0.07)	0.22 (0.10)	.477
	RA	0.19 (0.07)	0.21 (0.06)	0.19 (0.09)	.565
	Axial	1.84 (0.34)	1.68 (0.32)	1.78 (0.34)	.181
	Radial	1.33 (0.35)	1.16 (0.26)	1.32 (0.41)	.099
	ADC	1.50 (0.34)	1.33 (0.27)	1.47 (0.38)	.095
Posterior[b]	FA	0.22 (0.08)	0.25 (0.05)	0.23 (0.10)	.635
	RA	0.19 (0.07)	0.21 (0.05)	0.19 (0.09)	.695
	Axial	1.82 (0.36)	1.68 (0.33)	1.76 (0.34)	.439
	Radial	1.35 (0.36)	1.18 (0.28)	1.32 (0.41)	.261
	ADC	1.51 (0.35)	1.34 (0.29)	1.47 (0.38)	.266
Optic radiation[b]	FA	0.32 (0.05)	0.34 (0.06)	0.29 (0.08)	.045[c]
	RA	0.27 (0.04)	0.29 (0.05)	0.25 (0.07)	.032[c]
	Axial	2.07 (0.32)	1.95 (0.34)	2.05 (0.32)	.387
	Radial	1.26 (0.24)	1.15 (0.24)	1.30 (0.26)	.162
	ADC	1.53 (0.26)	1.41 (0.26)	1.54 (.26)	.243
Deep white matter					
Posterior limb internal capsule[b]	FA	0.50 (0.07)	0.51 (0.04)	0.48 (0.09)	.361
	RA	0.46 (0.07)	0.47 (0.05)	0.44 (0.10)	.434
	Axial	1.87 (0.27)	1.73 (0.26)	1.76 (0.28)	.141
	Radial	0.78 (0.15)	0.72 (0.13)	0.77 (0.17)	.352
	ADC	1.14 (0.17)	1.06 (0.18)	1.10 (0.19)	.289
Genu	FA	0.50 (0.07)	0.53 (0.06)	0.44 (0.10)	.001[c]
	RA	0.46 (0.08)	0.49 (0.07)	0.40 (0.10)	.002[c]
	Axial	2.27 (0.34)	2.13 (0.34)	2.20 (0.34)	.332
	Radial	0.97 (0.22)	0.85 (0.18)	1.07 (0.24)	.004[c]
	ADC	1.41 (0.24)	1.29 (0.22)	1.45 (0.25)	.075
Splenium	FA	0.54 (0.09)	0.59 (0.07)	0.46 (0.12)	.00001[c]
	RA	0.50 (0.10)	0.57 (0.08)	0.42 (0.13)	.00003[c]
	Axial	2.32 (0.34)	2.20 (0.34)	2.23 (0.35)	.615
	Radial	0.91 (0.20)	0.77 (0.17)	1.02 (0.22)	.00008[d]
	ADC	1.38 (0.22)	1.24 (0.21)	1.42 (0.21)	.012

Note:—RA indicates radial diffusivity.

[a] ANOVA *P* value ≤.005 significant.

[b] Measurements are average of left and right readings.

Tukey pair-wise comparisons:

[c] Term controls significantly different from neonates with CHDs; 2 other pair-wise comparisons (term controls versus preterm controls, preterm controls versus neonates with CHDs) nonsignificant.

[d] Neonates with CHDs significantly different from both preterm and term controls. Pair-wise comparison of preterm and term controls nonsignificant.

microstructural abnormalities in the splenium, suggesting some concordance between the techniques, but also enhanced sensitivity in the voxelwise analysis. (Furthermore, it should be noted that the statistical comparisons differed among the 2 techniques, with the TBSS technique only allowing comparisons among 2 groups, whereas the ROI-based method allowed for 3-way comparisons with the use of ANOVA). Because the TBSS technique is not adequate for measurement in gray matter structures, we used our ROI measurements for quantitative analysis of the thalamus, basal ganglia, and parietal-occipital gray matter.

Secondary Analytic Technique for Postprocessing DTI Data: Manually placed ROIs

DTI analysis was performed off-line with the use of DTIStudio . Diffusivity and anisotropy metrics were measured in a total of 11

standardized bilateral ROIs[1] chosen because they 1) allowed us to validate a portion of the TBSS analysis, which has been only recently applied to neonatal datasets, and 2) allowed us to assess group differences in structures where there was low anisotropy (ie, peripheral white matter regions) which the TBSS analysis was not well suited to address; and 3) allowed us to assess how our comparison cohorts of critically ill preterm and term neonates without CHD compared with other populations of "healthy" preterm and term infants.

Specifically, the manually delineated regions included 3 gray matter structures: thalamus, putamen, and occipital-parietal gray matter (all of which were marked on a single axial section at the level of the thalamus and genu/splenium of the callosum; the gray matter ROI measurements will be the subject of a forthcoming manuscript and will be published separately, and the data for these ROIs are not included); and 8 white matter structures: optic radiations, frontal and parietal periventricular cross-roads (a region known to be commonly affected by pWML or periventricular leukomalacia involving intersections between longitudinal cortico-cortical tracts in anterior-posterior and left-right orientation and thalamocortical tracts radiating centrally toward the peripheral cortex), posterior limb of the internal capsule, genu and splenium of the corpus callosum, and the corona radiata in the frontal, central (sensorimotor), and parietal regions. Standardized axial sections were used for all ROIs. In cases of head tilt, ROIs were delineated at multiple section levels and then averaged. For structures such as the thalamus and putamen, ROIs were drawn so as to outline the structure. For other ROIs, a standardized circular ROI of a given diameter was used. The senior neuroradiologist (A.P.) ensured consistency of positioning for all regions. In all regions, fractional anisotropy (FA), eigenvalue 1 (λ_1), eigenvalue 2

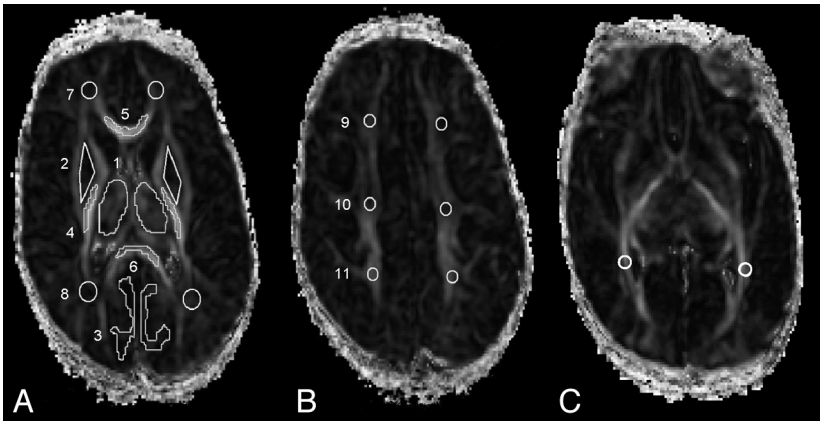

ON-LINE APPENDIX FIG. 1. *A*, Level showing the bilateral ROI's deep gray matter and certain white matter structures: GM: (1) thalamus, (2) putamen, (3) cortical occipital parietal GM; WM: (4) posterior limb of internal capsule, (5) genu, (6) splenium, (7) frontal WM, (8) occipital parietal posterior WM; *B*, Level of the centrum semiovale showing deep white matter structures; (9) anterior WM, (10) sensorimotor WM, (11) posterior WM.

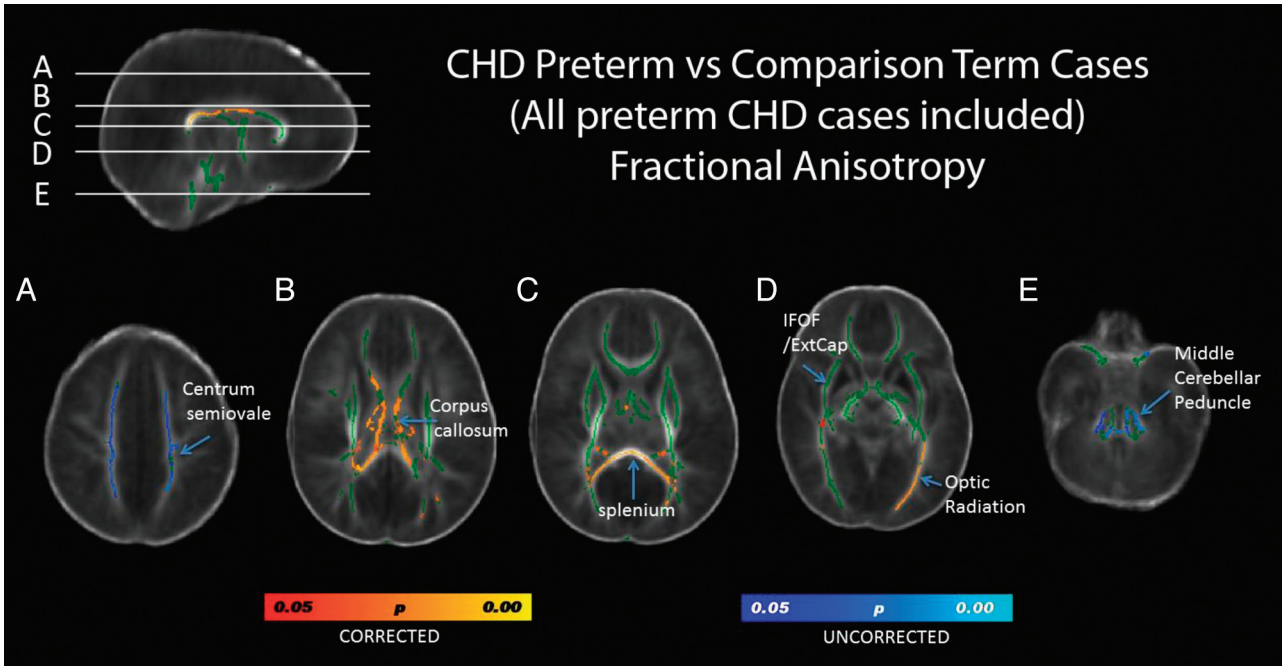

ON-LINE APPENDIX FIG. 2. Compared to the term neonates without CHD, the preterm CHD neonates were found to have significantly reduced FA in focal regions of the posterior cerebral white matter. This included key regions caudally within the developing visual system (ie, optic radiations and the splenium of the corpus callosum) with relative sparing of the more rostral visual areas (ie, the inferior frontal-occipital fasciculus).

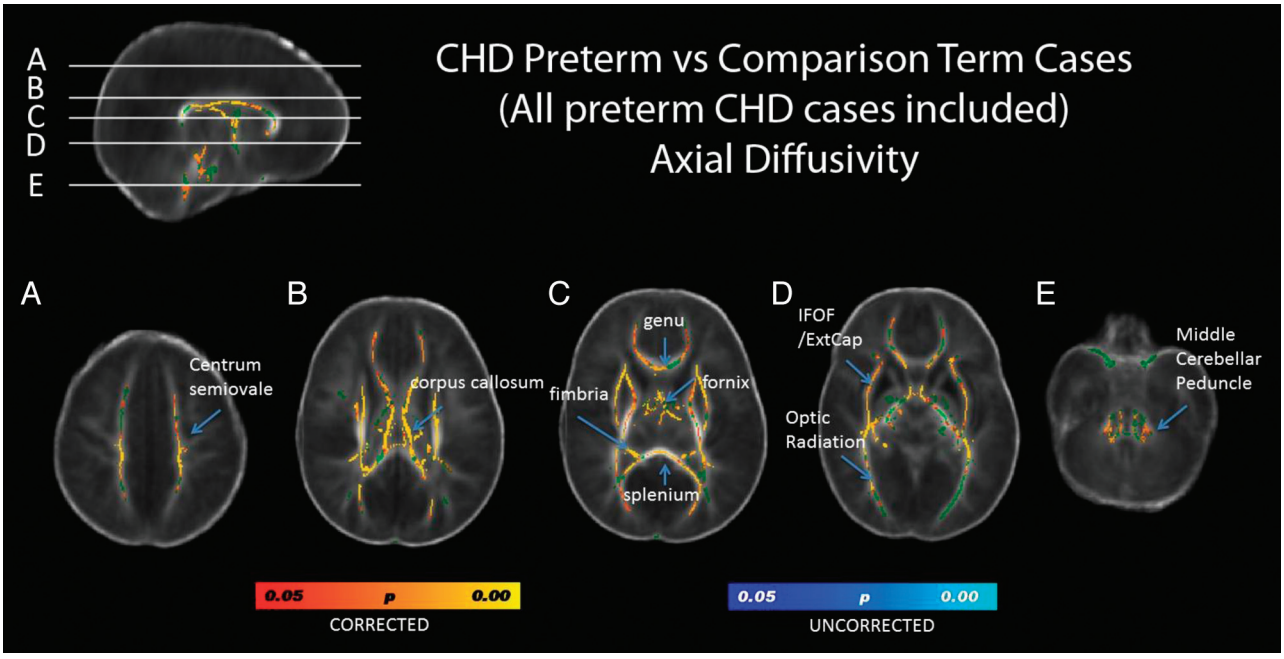

ON-LINE APPENDIX FIG. 3. In contrast with the FA results, changes in diffusivity, including increases in both axial diffusivity and radial diffusivity, were observed in widespread cerebral white matter regions in the preterm neonates with CHD. There was involvement of all neural systems noted including both rostral and caudal visual areas, the limbic system, the motor system and frontal lobe regions.

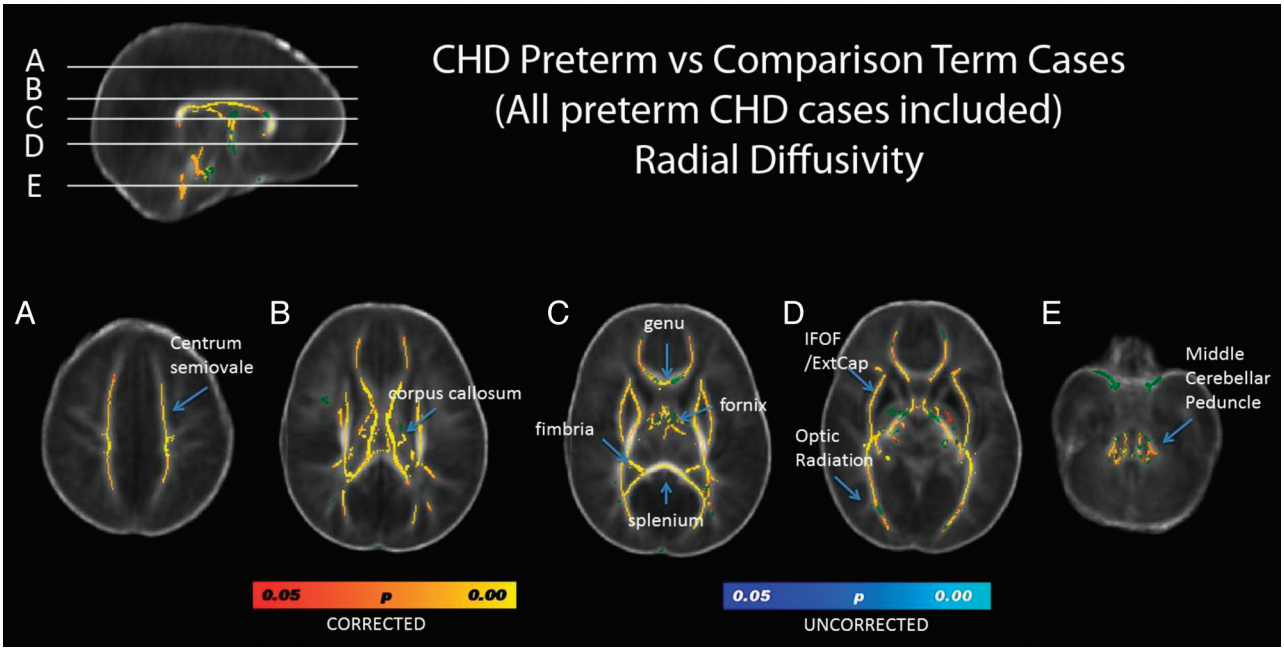

ON-LINE APPENDIX FIG. 4. In contrast with the FA results, changes in diffusivity, including increases in both axial diffusivity and radial diffusivity, were observed in widespread cerebral white matter regions in the preterm neonates with CHD. There was involvement of all neural systems noted including both rostral and caudal visual areas, the limbic system, the motor system and frontal lobe regions.

(λ_2), eigenvalue 3 (λ_3), and mean diffusivity were calculated. Eigenvalue 1 was also considered as axial diffusivity (λ_{11}) . Radial diffusivity ($\lambda\perp$) was calculated as the average of eigenvalues 2 and 3.

ROI Placement

On-line Appendix Fig 1 shows *A*, Level showing the bilateral ROI deep gray matter and certain white matter structures: Gray matter: *(1)* thalamus, *(2)* putamen, *(3)* cortical occipital parietal GM; white matter: *(4)* posterior limb of internal capsule, *(5)* genu, *(6)* splenium, *(7)* frontal WM, *(8)* occipital parietal posterior WM. *B*, Level of the centrum semiovale showing deep white matter structures: *(9)* anterior WM, *(10)* sensorimotor WM, *(11)* posterior WM.

Supplementary Results

TBSS Results (All Anatomic Levels): Preterm CHD versus term controls (before cases with pWMLs were removed). On-line Appendix Figs 2–4.

Results: DTI—Manual ROIs

In relation to the 3-way comparisons, significant differences in fractional anisotropy and radial diffusivity among the groups were detected again in the visual system (optic radiations, splenium of the corpus callosum), and in a frontal region (ie, the genu of the corpus callosum). Pair-wise comparisons demonstrated that for the optic radiations and the genu, patients with CHD had significantly lower FA and increased RD compared with term neonates. Additionally, in the splenium, FA was lower in the patients with CHD compared with term neonates, whereas RD was increased relative to the term and preterm neonates. Finally, differences in axial diffusivity were detected in the thalamus, with the term comparison group showing lower axial diffusivity values than the patients with CHD or preterm comparison group. There was strong correlation between both the TBSS analysis and ROI analysis in that microstructural abnormalities were emphasized in the splenium with the use of either technique. The differences seen between these 2 techniques probably are related to the difference in FA skeleton generation and signal-to-noise ratio generated from ROI analysis. The results indicated that the DTI measurements in this study for our term and preterm cases without CHD are within range of published normative data.[1]

REFERENCES

1. Bartha AI, Yap KR, Miller SP, et al. **The normal neonatal brain: MR imaging, diffusion tensor imaging, and 3D MR spectroscopy in healthy term neonates.** *AJNR Am J Neuroradiol* 2007;28:1015–21
2. Ball G, Counsell SJ, Anjari M, et al. **An optimised tract-based spatial statistics protocol for neonates: applications to prematurity and chronic lung disease.** *Neuroimage* 2010;53:94–102